ISBN: 978-3-95450-249-3 ISSN: 2673-5350 doi: 10.18429/JACoW-IBIC2024-WEP39

THE DEVELOPMENT OF BUNCH-BY-BUNCH TRANSVERSE FEEDBACK SYSTEM AT SSRF BASED ON RF DIRECT SAMPLING*

J. L. Pan, Shanghai Institute of Applied Physics, Chinese Academy of Sciences, Shanghai, China
also at University of Chinese Academy of Sciences, Beijing, China
L. W. Lai†, Y. M. Zhou, Shanghai Advanced Research Institute, Chinese Academy of Sciences, Shanghai, China

Abstract

The commonly used bunch-by-bunch transverse feedback system (TFB) is based on the scheme of analog downconversion, which down converts the $3\times f_{RF}$ beam signal to the baseband with a phase adjusted local oscillator. The system contains a large number of analog devices, which make the system complex. Today, sampling the high frequency signal directly with high performance ADC is available. A new bunch-by-bunch TFB based on RF direct sampling is under development at SSRF. The new system structure is much simpler compared to the traditional one and much powerful. The direct sampling processor has 4 input channels, which can simultaneously process horizontal, vertical, large bunch vertical feedback, and bunch charge measurement. The RF processor has 4 ADC channels (maximum sampling rate is 2.6GHz, bandwidth is 9GHz), 4 DAC channels (maximum frequency 500MHz). The processor uses Xilinx system-on-chip UltraScale+ MPSoC FPGA. Paper will introduce the system structure, the processor design and performance.

INTRODUCTION

The Shanghai Synchrotron Radiation Facility (SSRF) is a third-generation medium-energy synchrotron radiation source, which was completed in 2009. It operates with a beam energy of 3.5 GeV, a storage ring circumference of 432 meters, a harmonic number of 720, and an RF frequency of 499.654 MHz.

For a synchrotron radiation source, the quality of the beam is a key factor in evaluating its performance. The electron beam circulating in the storage ring is influenced by various complex physical factors, including higher-order modes in RF cavities, resistive wall impedance, ion instability, and multi-bunch coupling. These instabilities can collectively cause the beam to deviate from its designed trajectory, increase emittance, shorten beam lifetime, and affect the operational stability and light quality. The TFB is a critical system used for controlling beam stability in synchrotron light sources. By monitoring the beam's motion in real-time and applying feedback control, the system can effectively suppress unstable modes and maintain transverse beam stability. The main components of the TFB include the Beam Position Monitor (BPM), transverse feedback electronics, power amplifiers, and kickers. Among these, the TFB electronics, which convert the detected beam position offset signals into feedback signals, are at the core of the system.

In the early stages, due to the limitations of ADCs and processors, it was not possible to directly sample high-frequency signals, so the transverse feedback system had to perform analog downconversion before signal sampling. The first-generation transverse feedback electronics at SSRF used the sum signal from the four BPM channels as the local oscillator to downconvert the frequency band around 1.5 GHz to the baseband. Additionally, four ADCs with a sampling frequency of 125 MHz were used for delayed sampling, achieving a 500 MHz sampling rate for single-point sampling of each bunch. Starting in December 2016, as part of the Phase II upgrade project at SSRF, the beam measurement system was upgraded [1, 2], including the replacement of the transverse feedback system with Dimtel iGp12 processor paired with FBE-LT front and back ends. The principle is as follows: The BPM output signals undergo sum and difference operations and are then passed through a bandpass filter with a center frequency of 1.5 GHz and a bandwidth of 500 MHz to extract the beam signal near the 3rd harmonic of the RF frequency. The machine clock is then multiplied to 1.5 GHz and used as the local oscillator to downconvert the filtered signal to the baseband. Finally, the beam position information is obtained by single-point sampling using a 500 MHz ADC, and the processor calculates the feedback signal based on the position information.

The RF front-end structure of such schemes is complex, with numerous analog components, making it susceptible to environmental changes. Moreover, due to single-point sampling, it is prone to longitudinal oscillation effects. Additionally, in the Phase II project of SSRF, an additional feedback loop was added to handle vertical oscillations of large bunches, on top of the existing horizontal and vertical feedback loops. However, since one processor can only handle feedback for one direction, the cost is relatively high. Therefore, there is a need for new methods to address these issues.

RF DIRECT SAMPLING ELECTRONICS

In recent years, with advancements in technology, the performance of ADCs has significantly improved, making it possible to directly sample beam signals. For example, in the RF direct sampling bunch-by-bunch transverse feedback system at Spring-8, the system utilizes four ADCs with a sampling rate of 125 MHz and a bandwidth of 750

* Work supported by The National Science Foundation of China (Grant No.12175293). Youth Innovation Promotion Association, CAS (Grant No. 2019290). Outstanding member of the Youth Innovation Promotion Association, CAS. SHINE R&D and project. SSRF operation funding research project.
† Corresponding author: lailw@sari.ac.cn

ISBN: 978-3-95450-249-3 ISSN: 2673-5350 doi: 10.18429/JACoW-IBIC2024-WEP39

MHz to achieve a sampling rate of 500 MHz through delayed sampling [3]. In the multi-bunch feedback system at the Swiss Light Source (SLS), which is based on the RF System-on-Chip (RFSoC), the ADCs within the RFSoC, with a sampling rate of 4 GHz and a resolution of 12 bits, are used to directly sample the signals output by the BPM [4].

RF Direct Sampling Prototype

To evaluate the feasibility of the RF direct sampling transverse feedback scheme, we designed and developed an RF direct sampling prototype (RFDP) (as shown in Fig. 1). The processor is composed of an FPGA mainboard and an ADC sampling daughterboard, which are connected via an FMC interface and use the JESD204B communication protocol. The ADC sampling daughterboard includes four ADC channels, with the external clock being frequency-multiplied by the LMX2582 and LMK04832 to serve as the ADC sampling clock. The performance parameters of the RFDP are listed in Table 1.

Figure 1: RF Direct sampling prototype.

Table 1: Performance Parameters of the Prototype

Parameter	Value
Channels	4
Bandwidth	9 GHz
ADC bits	14
Max ADC rate	2.6 GHz
FPGA	Xilinx ZCU15EG
Clock	External
Trigger	Ext./Self/Period
SFP	2 UDP, 2Aurora
Interlock	Lemo
PL DDR4	2 GB
GPIO	12
Software	Arm-Linux/EPICS

RF Direct Sampling Beam Experiment

According to accelerator theory, the signal within the f_{RF} bandwidth, centered at integer multiples of the beam's RF frequency, contains all the transverse oscillation modes. To avoid aliasing during sampling, the signal needs to be filtered to extract a specific frequency band. Finally, to ensure the signal amplitude matches the ADC's dynamic range as closely as possible, the filtered signal must be amplified or attenuated as needed.

The power of the BPM A and C channel difference signals was measured at frequencies of f_{RF}、$2f_{RF}$、$3f_{RF}$、$4f_{RF}$, and $5f_{RF}$, as shown in Fig. 2. It is evident that within the range from f_{RF} to $4f_{RF}$, the power of the beam signal increases with frequency. Theoretically, selecting signals near $4f_{RF}$ can achieve the highest signal-to-noise ratio for the system. However, in practice, due to the clock jitter of the ADC sampling, additional noise is introduced, which leads to a reduction in the system's resolution.

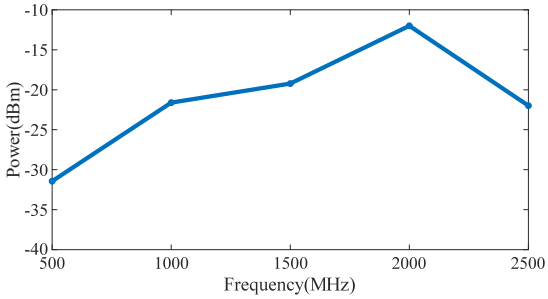

Figure 2: The amplitudes at different frequency points.

To validate the feasibility of the RF direct sampling scheme, we constructed an experimental platform as shown in Fig. 3. The A and C channel signals from the BPM are input into a 180° Hybrid module to calculate the difference signal. Since the A and C electrodes are on a diagonal of the BPM, the A-C signal simultaneously contains position data for both the horizontal and vertical directions. After filtering and amplification, the signal is sampled by the ADC. The processor is configured in a threshold-triggered sampling mode, with an ADC sampling frequency of 2 GHz, where each bunch corresponds to four sampling points. The ADC clock is synchronized with the machine clock, and the delay on the ADC clock signal cable is adjusted so that one of the sampling points aligns with the peak of the bipolar pulse. During the transient process after injection in Top-up mode, sampling is performed, and position data is calculated using the samples that fall on the peak.

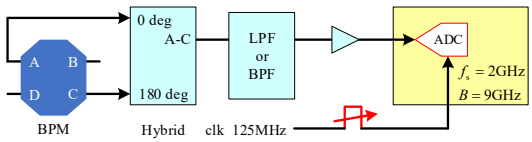

Figure 3: The verification test schematic of the RF direct sampling scheme.

The experimental platform was configured with different filters to extract signals from various frequency bands. We tested four types of filters: 580 MHz LPF, 700 MHz LPF, 780 MHz LPF, and 1.5 GHz BPF (B=500 MHz). Using the 1.5 GHz BPF (B=500 MHz) as an example, data was sampled over 4000 turns. The ADC data from the first turn is shown in Fig. 4, and the turn-by-turn (TbT) position variation for all bunches is illustrated in Fig. 5.

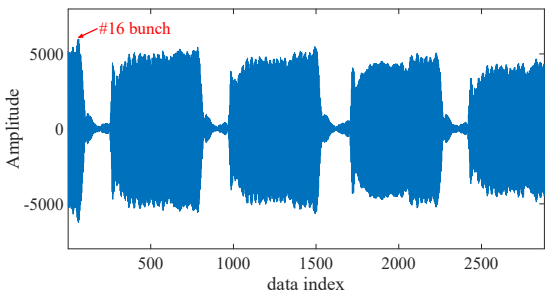

Figure 4: Raw ADC data (first turn).

ISBN: 978-3-95450-249-3 ISSN: 2673-5350 doi: 10.18429/JACoW-IBIC2024-WEP39

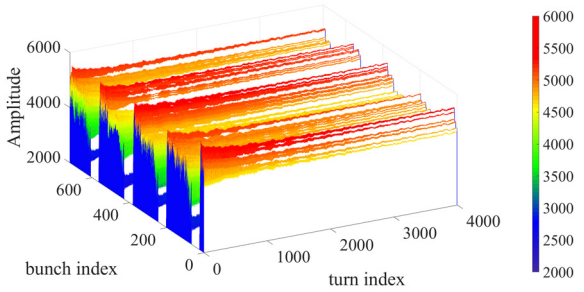

Figure 5: TbT position of all bunches.

Select the 16th bunch with the maximum amplitude in the A and C difference signals as the research subject. The time-domain waveform and frequency spectrum of its TbT position are shown in Fig. 6. The damping effect on the transverse oscillation after injection can be clearly observed, and the fractional parts of the tune values in the horizontal and vertical directions are 0.228 and 0.163, respectively. Figure 7 shows the TbT positions and frequency spectrum collected by the iGp12 TFB processor.

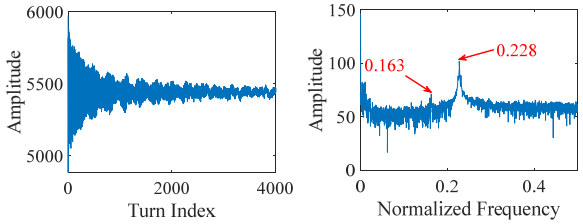

Figure 6: The TbT positions and frequency spectrum of the 16th bunch collected by RFDP.

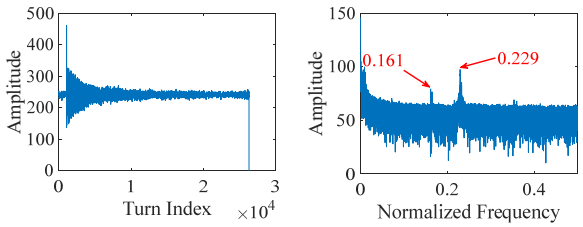

Figure 7: The TbT positions and frequency spectrum sample by the iGp12 TFB processor.

System Noise Evaluation

The noise of the entire system is evaluated using the Mode Independent Analysis (MIA) method. This method is commonly used for analyzing multi-turn position data in storage rings and allows for the separation of noise from the actual transverse motion of the beam, thereby extracting more useful information for accelerator physics research. The method is based on the principle of Singular Value Decomposition (SVD). For any real-valued matrix M , there exist orthogonal matrices U and V and a diagonal matrix S such that:

$$M = USV^T \tag{1}$$

In the above equation, M represents the matrix of bunch position data, with rows indexed by bunch number (1 to 720) and columns indexed by turn number (1 to 4000). The diagonal elements of S are singular values, which reflect the significance of each transverse oscillation mode within the overall transverse motion; larger values correspond to a higher proportion of the respective oscillation mode. The columns of U and the rows of V^T represent the time-domain characteristics and amplitude characteristics of the oscillations for each corresponding mode, respectively. In practical applications, it is necessary to first standardize the position data of each bunch so that the mean is 0 and the standard deviation is 1[5]. The standardized value of each element in the matrix M is given by:

$$M_{ij}^{std} = \frac{M_{ij} - \mu_i}{\sigma_i} \tag{2}$$

In the equation, μ_i denotes the mean of the turn-by-turn position data for each bunch, and σ_i denotes the standard deviation of the turn-by-turn position data for each bunch.

As shown in Fig. 8, the SVD of the A and C differential signals reveals the distribution of different modes. As the mode ID increases, the singular values rapidly decay, indicating that the transverse oscillations of the bunch are concentrated mainly in the first few modes. For the bunch numbered 16, the transverse oscillations of the first five modes are illustrated in Fig. 9.

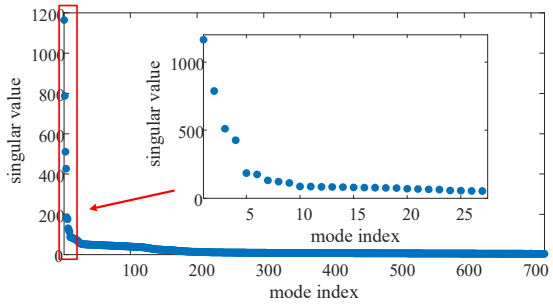

Figure 8: Distribution of singular values with mode ID.

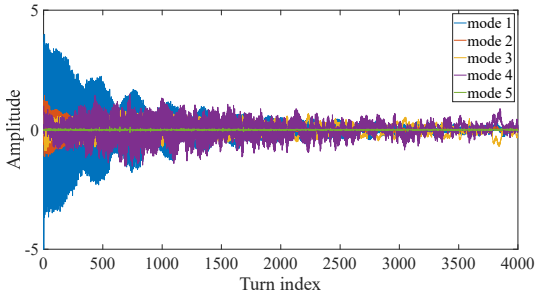

Figure 9: Transverse oscillations of the first five modes.

From Fig. 8, it can be seen that the transverse oscillation for Mode 5 is much smaller than that of the previous modes and does not show the decay process of oscillation. Therefore, starting from Mode 5 and beyond, all subsequent oscillation modes can be considered as system noise. By retaining the singular values of the first four modes and setting the singular values from Mode 4 to Mode 720 to zero, and then reconstructing the matrix using Equation (1), the transverse oscillation data excluding system noise can be obtained as shown in Fig. 10. It can be observed that after applying SVD and removing the noise modes, the noise

ISBN: 978-3-95450-249-3 ISSN: 2673-5350 doi: 10.18429/JACoW-IBIC2024-WEP39

content in the transverse oscillation data has significantly decreased.

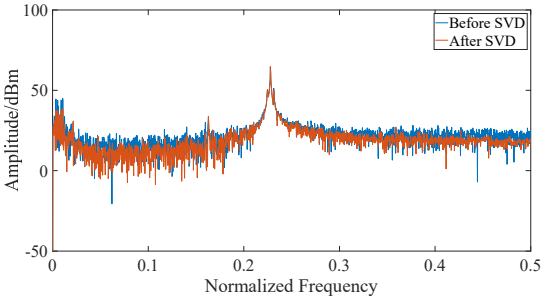

Figure 10: Transverse oscillation spectrum before and after SVD.

By retaining only the singular values corresponding to the noise modes and reconstructing the matrix, we obtain the system noise matrix. The standard deviations of the system noise are calculated for four different filter configurations: 580 MHz LPF, 700 MHz LPF, 780 MHz LPF, and 1.5 GHz BPF (B=500 MHz). The results are shown in Fig. 11.

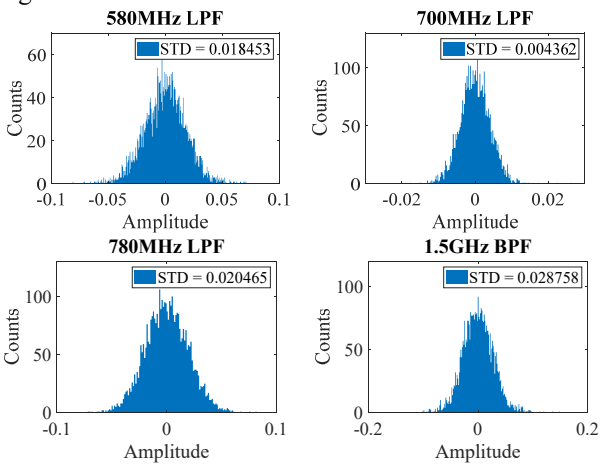

Figure 11: System noise distribution with different filters (peak value method).

It can be observed that the noise with a low-pass filter is lower than that with a band-pass filter. This is because the ADC is more sensitive to clock jitter and longitudinal oscillations of the bunches in band-pass undersampling mode. The same amount of clock jitter and oscillation introduces greater noise.

The aforementioned approach calculates the bunch position data using a single peak value point, which inherently makes it difficult to avoid noise introduced by clock jitter. Therefore, we consider an alternative method for computing position data: with an ADC sampling rate of 2 GHz, each bunch corresponds to 4 sampling points (V_1、V_2、V_3、V_4). The peak value of the bipolar pulse is obtained using Equation (3):

$$V_{\text{peak}} = \sqrt{V_1^2 + V_2^2 + V_3^2 + V_4^2} \tag{3}$$

Using the aforementioned method, the system noise was evaluated for several filters, and the results are shown in Fig. 12. It can be observed that the system noise is significantly reduced, indicating that calculating position data using the four-point method can substantially decrease the noise introduced by ADC clock jitter.

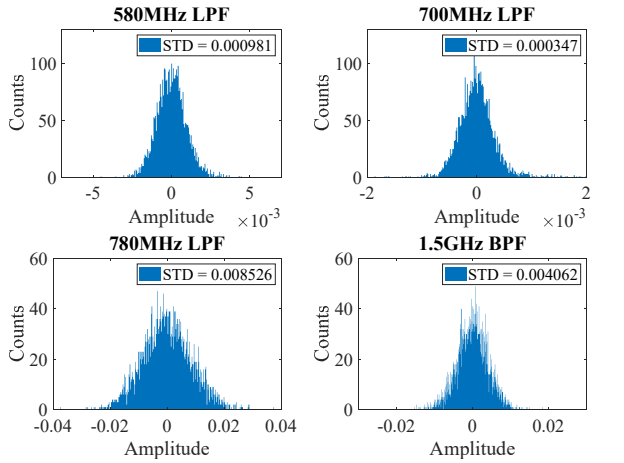

Figure 12: System noise distribution with different filters (four-point method).

CONCLUSION

The paper explores the use of RF direct sampling technology for transverse feedback signal processing, conducting experimental verification through an RF direct sampling prototype. The results show that the RF direct sampling scheme can measure the transverse oscillation and tune of the bunches, making it suitable for transverse feedback. A comparison of noise between peak sampling and four-point sampling methods demonstrates that the four-point method effectively reduces the impact of longitudinal jitter. Future work will focus on developing a complete transverse feedback processor and upper-level software based on these findings.

REFERENCES

[1] http://ssrf.sari.ac.cn/kydt/202404/t20240429_778684.html

[2] https://www.cas.cn/yw/202405/t20240515_5014804.shtml

[3] Nakamura, T., Z. R. Zhou and K. Kobayashi. “Bunch by Bunch Feedback by RF Direct Sampling”, in *Proc. EPAC08*, Genoa, Italy, p. 3287.

[4] P. H. Baeta Neves Diniz Santos, B. Keil, and G. Marinkovic, “RF System-on-Chip for Multi-Bunch and Filling-Pattern Feedbacks”, in *Proc. IBIC'22*, Kraków, Poland, Sep. 2022, pp. 379-382. doi:10.18429/JACoW-IBIC2022-WE2C4

[5] G. Kube, J. Neugebauer, and F. Schmidt- Föhre, “BPM Resolution Studies at PETRA III”, in *Proc. IBIC'19*, Malmö, Sweden, Sep. 2019, pp. 517-521. doi:10.18429/JACoW-IBIC2019-WEPP005